

## Examining the Impact of Conical Fin Shape on Hydrothermal Characteristics

Ehsan F. Abbas<sup>1\*</sup>, Atalah H. Jassim<sup>2</sup>, Thamer K. Salem<sup>2</sup>

<sup>1</sup>Engineering Technical College/ Kirkuk, Northern Technical University, Tikrit 34001, Iraq

<sup>2</sup>Engineering College, University of Mosul, Mosul 41003, Iraq

Corresponding Author Email: [ehsanfadhil@ntu.edu.iq](mailto:ehsanfadhil@ntu.edu.iq)



Copyright: ©2025 The authors. This article is published by IETA and is licensed under the CC BY 4.0 license (<http://creativecommons.org/licenses/by/4.0/>).

<https://doi.org/10.18280/ijht.430104>

### ABSTRACT

**Received:** 15 August 2024

**Revised:** 12 January 2025

**Accepted:** 27 January 2025

**Available online:** 28 February 2025

#### **Keywords:**

*heat sink, staggered fin arrangement, conical fin, truncated cone fin, steam condensation*

This study examined the transformation of cone fins into truncated cone fins under low laminar forced convection heat transfer, focusing on their effects on heat transfer and steam condensation in a staggered heat sink arrangement. It calculated the outlet cold water temperature and included five cone shapes based on the tip-to-base diameter ratio, ranging from 0 to 0.8 in increments of 0.2 while keeping the surface area, height, and transverse pitch constant. The results showed that using a truncated conical fin instead of a conical fin decreased heat transfer, the convection heat transfer coefficient, and the steam condensation rate. An increased tip diameter to base diameter ratio further reduced these parameters due to less contact area between the fin base and the plate surface. Additionally, there was strong agreement between theoretical and experimental methods in calculating the outlet water temperature and convection heat transfer coefficient. The DOE suggested optimal working conditions in every heat sink sample, and when their results were validated experimentally, it found good agreement. Additionally, the DOE provided empirical relations to determine heat transfer rate, pressure drop and steam condensation rate as a function of  $P_s$  and  $V_w$ .

## 1. INTRODUCTION

A heat sink is designed to effectively absorb or dissipate heat from its environment using extended surfaces, like fins and spines. These components are crucial in applications that require efficient heat management, such as refrigeration, heat engines, and cooling electronic devices. The typical design features a metal structure with several cooling fins called a fin array. To improve the heat sink's performance, one can increase the fins' thermal conductivity, surface area, or heat transfer coefficient. Longitudinal fins are available in various rectangular, triangular, and parabolic profiles. The rectangular profile is the simplest and most commonly used design, especially for multiple-fin arrays [1]. Many studies have been performed over three decades in order to optimize heat sink design, and optimization included fin dimensions, shape, material, arrangement, position, and fluid direction. The first one provided a mathematical analysis to design fin two centuries ago [2]. As documented by Harper et al. [2], the development of mathematical models for fin profiles aims to optimize material usage under specified conditions. This is mainly true when the fin's linear temperature gradient extends from the base to the tip [3]. The parameters for conical fins were established in previous study, and the heat dissipation rate is contingent upon the Biot modulus, which is determined by the base radius and the aspect ratio of the fin's height relative to its base radius [4]. Different fin shapes' temperature gradients and efficiency were derived mathematically [5, 6]. Murray-Gardner assumptions have been proposed to solve the

heat transfer equation for three distinct fin geometries: rectangular, triangular, and spinnable [7]. Researchers have worked on optimizing fins for heat transfer for nearly sixty years. While theoretically limitless performance can be envisioned, achieving it in practice is not feasible. However, designing fins within practical limits presents new opportunities for improving extended-surface heat transfer [8]. Razelos and Imre [9] studied minimizing mass with variable heat transfer coefficients using Pontryagin's maximum principle. The findings indicate that the final volume and width exhibit a distinct relationship with the material's thermal properties. Aziz and Beers-Green [10] optimized the rectangular fin for convection and radiation using Maple. They presented charts of optimum convection-conduction and radiation-conduction numbers for various Biot numbers and dimensionless temperatures. Hemptid and Kittichaikarn [11] investigated various design parameters and flow directions to assess micro-heat sink performance. They found optimal thermal performance with the V-type model at  $75^\circ$  and a distance of 2.5 mm from the heat sink front to the inlet and outlet centerline. Peng et al. [12] investigated the heat transfer and flow characteristics associated with multi-jet microchannel heat sinks. Employing the SIMPLE-type finite volume method, they performed a numerical simulation of the three-dimensional flow and transfer processes inherent to the heat sink. They also performed a numerical study on how fan position affects the thermal efficiency of an elliptical pin-fin heat sink. They examined two fan positions: one positioned outside the heat sink and another located within a cut-out

template. The study included simulations for Re numbers ranging from 3400 to 16000 and  $q''$  values from 104 to  $4 \times 10^5$  kW/m<sup>2</sup>. The results showed that the second model outperformed the first. Sehgal et al. [13] investigated how different flow arrangements affect microchannel heat sinks' heat transfer and flow characteristics. They examined U-type, S-type, and P-type flow arrangements. Experiments used Re numbers from 220 to 1100 and electric power from 100 to 800 W. They observed the best thermal performance in this type and the highest pressure drop when compared to the other types. Babar et al. [14] investigated the thermal performance of airfoil fin-shaped heat sinks by evaluating both inline and staggered fin configurations. The experiments varied the Re number from 600 to 680 and the power input from 75 to 125 W. It was observed that the Nu number of an inline arrangement is more significant; however, the overall thermal performance of staggered arrangements is better. Leon et al. [15] employed numerical techniques to explore how aerodynamic shaping affects the cooling fan in a staggered fin heat exchanger. Their findings indicated that a rounded staggered configuration dissipates heat at 33.3% lower airspeed than an in-line fan. Abuska and Çorumlu [16] used experimental methods and forced convection to study the thermal behavior of a staggered cone-[in-fin] (CPFHS<sub>ST</sub>) with a modified staggered layout. The modified samples include CPFHS<sub>MST</sub>, CCPFHS<sub>PAR</sub>, and CCPFHS<sub>PERP</sub>. The CPFHS<sub>MST</sub> demonstrated superior thermal performance compared to CPHS<sub>ST</sub>, CCPFHS<sub>PER</sub>, and CCPFHS<sub>PERP</sub>, exceeding them by 10.9%, 12%, and 13.3%, respectively. optimized [in-fin] heat sinks with in-line and staggered arrangements. They studied hydrothermal characteristics at Re numbers from 100 to 2000, applying a constant heat flux of 100 W/m<sup>2</sup>. The properties of the Al<sub>2</sub>O<sub>3</sub>-water nanofluid were as follows:  $\rho$  of 1027.9 kg/m<sup>3</sup>,  $cp$  of 4.05 kJ/kg·K, and  $k$  of 0.62 W/m·K. The CuO-water nanofluid, the properties were:  $\rho$  of 1038.1 kg/m<sup>3</sup>,  $cp$  of 3.767 kJ/kg·K, and  $k$  of 0.637 W/m·K. The results indicated that the staggered arrangement was better than an in-line arrangement by 19%, enhancing heat transfer but increasing pressure drop by 79%. Yoo et al. [17] investigated the theoretical thermal properties of a staggered tube bank in crossflow. Tube spacing, location, and Re numbers were studied to evaluate the  $h_x$ . They observed that the average Nu number increased by 30% and 65% in the second and third rows compared to the first row. Achenbach [18] investigated the  $\Delta P$  and  $h$  in smooth, rough, and staggered bank tubes within high Re number crossflow. He studied hydrothermal characteristics at a Re number ranging from  $4 \times 10^4$  to  $7 \times 10^6$ , with an air pressure of 40 bar and a maximum roughness of 0.009. It shows that the flow and heat transfer in a staggered tube bundle resemble those in a single cylinder in cross-flow. A critical Re number signals the transition from laminar to turbulent flow, affected by surface roughness. Beyond this point, turbulent enthalpy exchange enhances heat transfer, indicating that bluff body flow characteristics are more effective and important. John et al. [19] conducted a study examining the influence of fin shape on the overall thermal performance of a staggered microchannel heat sink. The investigation encompassed six distinct fin shapes: Square, triangular, circular, rhombic, rectangular, and elliptic. Experiments were carried out across Re numbers ranging from 50 to 500. The findings suggest that the circular fin heat sink exhibits superior thermal performance at lower Re < 200 compared to alternative designs. Tekale et al. [20] examined heat transfer in cylindrical and perforated fins arranged inline and staggered within a

rectangular channel, with a Re number of 13,500-42,000, clearance ratios  $d/L$  of 0, 0.33 and 1, and inter-fin spacing ratios  $X_t/X_l$  of 1.944 and 3.417. Their analysis indicates that perforated fins enhance heat transfer more effectively than solid fins, depending on clearance and inter-fin spacing ratios. Maji et al. [21] conducted a numerical investigation into improving heat transfer in perforated fin heat sinks arranged in inline and staggered configurations. Their findings indicated that the heat dissipation from the perforated fins surpassed that of the solid fins. Furthermore, the staggered arrangement demonstrated superior heat transfer enhancement compared to the inline configuration. Choudhary et al. [22] experimentally investigation into the thermal enhancement of a pin-fin heat sink equipped with a wing under forced convection. They explored inline and staggered configurations to understand better how airflow behaves around fins, with and without wings. They conducted experiments by varying the Re numbers from 6800 to 15100 and adjusting the ratios of  $X_t/X_l$  and  $L/d$ . The results indicated that heat transfer and pressure drop increased when  $X_t/X_l$  and  $L/d$  decreased. However, the researchers found that the optimum thermal performance for the pins with wings occurred when both  $X_t/X_l$  and  $L/d$  were equal to 2. bin Samsudin et al. [23] investigated the impact of adding wings to [in-fins] on the heat sink thermal performance. The four heat sink models illustrated in Figure 1 have been utilized. The results indicated that incorporating wings into fins enhances thermal performance by 47% for PHPFHSW compared to PHPFHS. Pressure drops for CPFHSW and CPFHS were 110 Pa and 23 Pa, respectively, at 5 m/s.

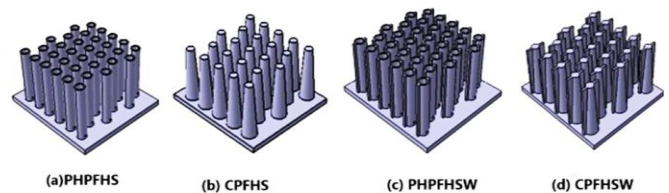


**Figure 1.** A diagram of the heat sink models that were utilized [23]

Abdelmohimen et al. [24] numerically investigation into the enhancement of heat dissipation by adding wings to pin-fin heat sinks at various angles. Five angles between 0° and 90° and Re numbers from 13500 to 37500 were simulated using both in-line and staggered arrangements. They found that a 0° inline arrangement produced the maximum number, while a staggered arrangement produced the maximum number at 22.5° however, both arrangements produced the maximum pressure drop at 0°. Qi et al. [25] conducted a numerical study on the thermohydraulic performance of interrupted flying wing fins (IFWF). The simulation considered the impact of fin geometry across different Re numbers ranging from 600 to 1600. Qi et al. [25] conducted a numerical study to investigate the thermohydraulic behaviors of interrupted flying wing-fins (IFWF). The simulation analyzed the impacts of fin geometry across different Re numbers, ranging from 600 to 1600. They utilized the response surface method to derive correlations for the j-factor and f-factor. The findings revealed that, at a Re number of 1000, the interruption has the most significant impact on the j-factor, f-factor, and j/f-factor. Massoudi and Hamida [26] examined the impact of combined wave wang fins and nanofluids on the thermal performance of fins. The study utilized two different heat samples: the first sample

featured rectangular wings on all four sides to support the square fin, while the second sample had wavy rectangular wings. The thermal efficiency of the aforementioned samples was assessed based on the length of the wings, the quantity of wind waves, and the angle of inclination of the heat sink box. Haque et al. [27] performed a numerical study to explore how fin shape affects the thermohydraulic properties of heat sinks. The simulation involved three fin shapes: cylindrical, twisted, and grooved, illustrated in Figure 2. Findings revealed that the grooved, circular perforated heat sink increased the average Nu number by 32% and boosted thermal performance by 27%.

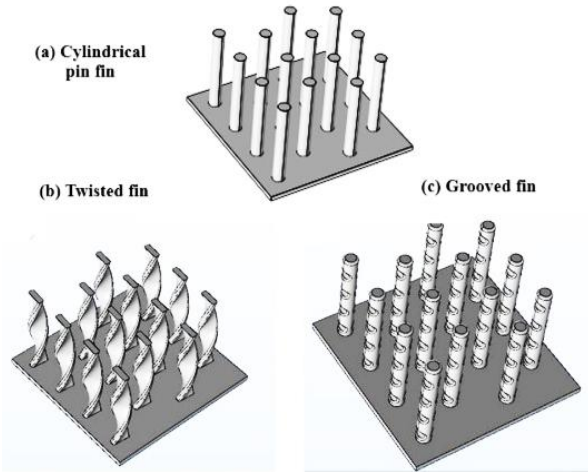


**Figure 2.** Types of heat sinks used [27]

Miao et al. [28] studied heat transfer and pressure drop from sine-wave flying wing fins (SWFWF) using design parameters such as the fin pitch-to-height ratio, height-to-wavelength ratio, amplitude-to-pitch ratio, and inclined angle. Optimization simulations were based on the *j* and *f* factors, showing average deviations of 0.85% for *j* and 4.9% for *f*. This study also examined the conical fin shape's effect on a heat sink's thermal performance in condensing steam. Recently, many studies have examined the thermal performance of conical-finned heat sinks, such as Çorumlu [29] investigated the effect of input power and ambient temperature on convection heat transfer coefficients. At an input power of 16.5 W, the Nusselt number increases as the ambient temperature rises. However, at 33 W, the opposite trend was observed. Ho and Leong [30] explored various fin shapes used in steam condensing, such as conical, sinusoidal, and cylindrical pin heat sinks. Their findings revealed that the conical fin demonstrated a superior condensation efficiency compared to the others, highlighting its effectiveness in this application. Haghghi et al. [31] compared heat transfer coefficients among four types of heat sinks: rectangular, circular, conical, and simple fin designs. The study incorporated configurations with 5, 7, and 9 fins for each heat sink type. Notably, the plate-fin heat sink design demonstrated the lowest thermal resistance, attributable to its increased surface area in contact with the airflow. Jaiswal [32] conducted a comparative analysis of the thermal performance of cylindrical and conical fins. Both types of fins possessed identical diameters and heights and were fabricated from the same material. The experimental procedures were executed under consistent working conditions involving free convection heat transfer. The findings indicated that while the cylindrical profile demonstrated superior effectiveness, its efficiency was relatively low. In contrast, the conical fins exhibited the

highest efficiency yet displayed significantly diminished effectiveness. Souida et al. [33] studied the effect of conical fin shape on the heat transfer coefficient (*h*) with height-to-diameter (*H/d*) ratios from 0.167 to 0.833 and *Re* numbers up to 8000. They found conical fins had higher hydrothermal performance factor (HPF) values than cylindrical fins, which increased as the *H/d* ratio decreased. The highest HPF value, 1.51, was achieved with *l/d*=0.167 at *Re* of 8,000. Pati et al. [34] performed a numerical comparison of fin geometries in inline and staggered configurations using Ansys Fluent. The study analyzed the *Re* number, interspacing ratio, and fin type on heat dissipation rates. They used cylindrical and conical fins of the same effective lengths in both arrangements. Results showed significant heat transfer improvement for staggered arrangements, which is ideal for low-*Re* micro heat transfer applications. An increase in the *Nu* number was observed, followed by a corresponding increase in the *Re* number for each arrangement. The studies reviewed focused on comparing the thermal performance of various fin shapes and the conical fin. Previous studies evaluated the influence of the fin height-to-diameter ratio and the fin arrangement on the operational conditions of heat transfer via free and forced convection. Conversely, the present study investigates the heat flux, pressure drop, quantity of steam condensation, and the *Nu* number of staggered conical finned heat sinks featuring various fin geometries, including conical and truncated conical fins, under forced convection. In contrast to prior research, this study maintains design parameters such as height, surface area, and transverse pitch at constant levels.

## 2. EXPERIMENTAL SETUP

A test rig containing many principal equipment and measurement devices, shown in Figure 3, was designed to execute the requested experiments in this study.

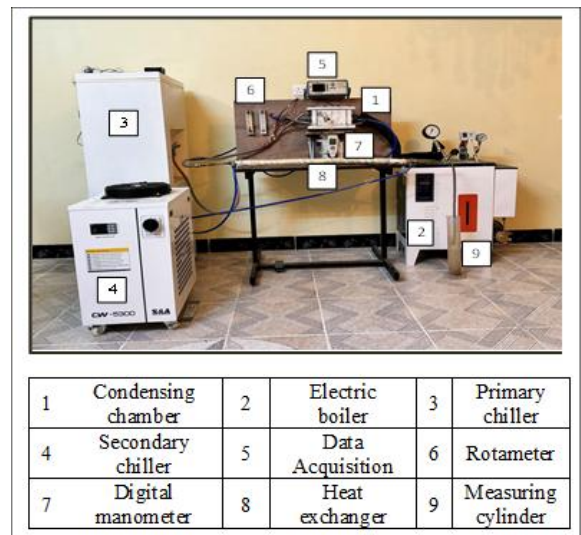


**Figure 3.** Photo of the test rig used

### 2.1 Test reg description

The test rig features a primary condensing chamber (CCH) constructed from thermal Teflon plates. The chamber has the following dimensions: (length of 220 × width of 190 × height of 110) mm. The wall thickness is 32 mm for the cold-water section and 25 mm for the condensation section. Additionally,

there are five holes of 14 mm in diameter. The cold-water and steam sections use four holes for the inlet and outlet of water and steam. In contrast, the fifth hole discharges the condensed steam upon completion of the experiment, as illustrated in Figure 4. It is also included in many accessory devices, such as the primary chiller, which is used for condensing steam in the CCH; the secondary chiller, which supplies chilled water to a heat exchanger with concentrated double pipes to condense steam that exits from the CCH; and the electric boiler, which generates steam with a maximum mass flow rate of 8 kg/hr at a temperature of 171°C and a pressure ranging from 0.4 to 0.7 MPa. Numerous measurement instruments have been employed to record experimental data, such as the data acquisition device Applent (AT4516), which was used to monitor temperatures in 16 locations via type T thermocouples, as illustrated in Figure 5. To regulate water flow into the CCH, a rotameter-type ASZ, adjustable for flow rates from 0.5 to 4 LPM, was utilized. A digital manometer was utilized to measure the  $\Delta P$  across a CCH, and measurement cylinders scaled the condensing steam in the CCH and the double-pipe heat exchanger.

## 2.2 Heat sink fabrication

This heat sink has a base plate that measures 176 mm × 140 mm × 3 mm. Equipped with 21 conical fins, each 10 mm in diameter and 60 mm long, the base plate and fins are made from a copper alloy of 94.8% copper and 4.8% aluminum. A heat sink was designed to allow fins to be easily replaced by fixing them to the base plate with screws. The heat sink was built with staggered fins, with an  $X_t$  of 30mm and an  $X_l$  of 26mm. Additionally, 21 M4 screws were brazed at the fin locations, as illustrated in Figure 6. Five sets of conical fins were manufactured with identical height and lateral surface area. The tip-to-base diameter ratio ( $\beta$ ) varied from 0 to 0.8 in increments of 0.2. Table 1 presents the specific dimensions for each set, and Figure 7 includes both a photo and a sketch of the fins. The cold coolant system (CCH) was designed to allow cold water to flow over the finned side while steam flows over the backside of the heat sink. To ensure a tight fit, we installed the heat sink securely in the CCH by placing a gasket between it and its guide.

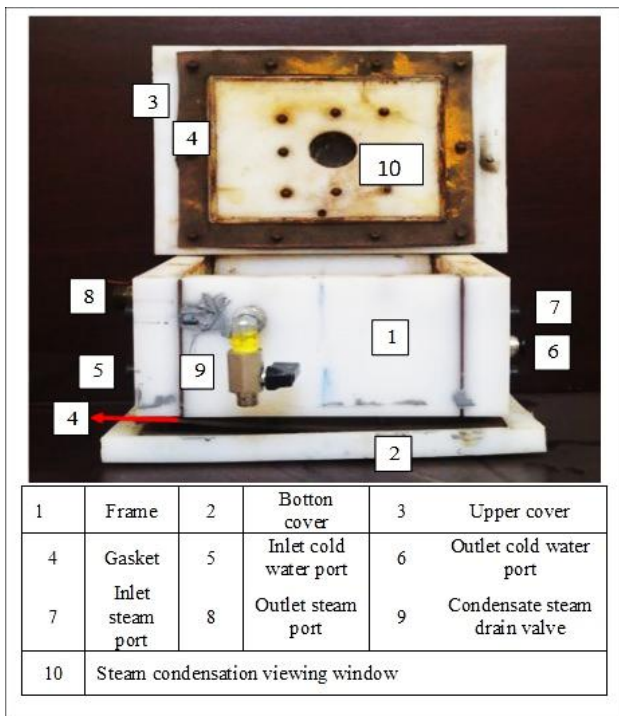


Figure 4. Photo of condensation chamber

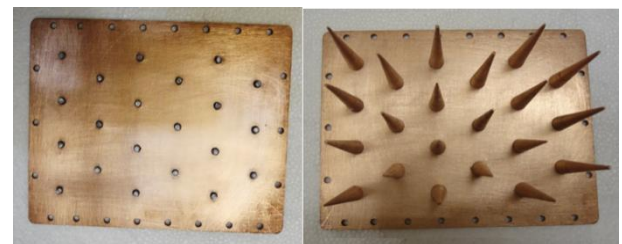


Figure 6. Photo of base plate and conical finned heat sink

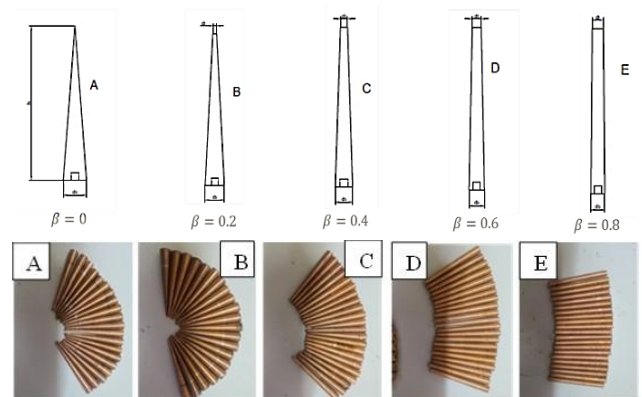


Figure 7. Schematic diagram and photos of the fins used

Table 1. Dimensions of fins used

Fin Symbol	$\beta$	$d_b$ , mm	$d_t$ , mm	$l$ , mm
A	0	10	0	60
B	0.2	8.38	1.64	60
C	0.4	7.16	2.846	60
D	0.6	6.27	3.76	60
E	0.8	5.57	4.456	60

## 2.3 Experimental design

The experiments were designed using Minitab software to optimize the thermal performance of the current test setup. We determined the necessary number of experiments by analyzing the response surface from the Design of Experiments (DOE) method in Minitab, considering the input variables  $P_s$  and  $V_w$ . The range for  $P_s$  is 2000 to 10000 Pa (gauge); for  $V_w$ , it is 0.5

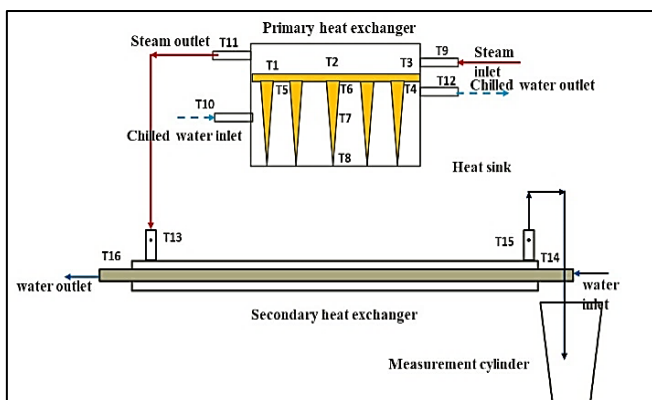


Figure 5. Schematic diagram of thermocouple locations in the test rig

to 2 LPM. The simulation resulted in four experiments at cubic points, five at center points in a cube, and four at axial points. Therefore, the total number of requested experiments is thirteen, which should be performed, as shown in Table 2. Initially, the steam was generated at the requested pressure for each working condition. Cold water was supplied to the CCH at a specified volume flow rate until the heat sink reached a steady state, and then steam was started to be supplied to the CCH for 10 minutes. Every minute, 16 temperatures in the test rig and pressure drop across CCH were recorded. At the end of the experiment, the condensing steam in the CCH and the exit steam, which condensed in the double-pipe heat exchanger, were measured.

**Table 2.** Details of the working conditions which the DOE designed for experiments

Working Conditions		Number of Experiments	Symbols
P <sub>s</sub> (Pa gauge)	V <sub>w</sub> (LPM)		
500	1.25	1	P1V2
2000	0.5	1	P2V1
2000	2.0	1	P2V3
6000	0.5	1	P3V1
6000	1.25	5	P3V2
6000	2.25	1	P3V4
10000	0.5	1	P4V1
10000	2.0	1	P4V3
11500	1.25	1	P5V2

### 3. CALCULATIONS

The experimental heat transfer rate dissipated to cold water from the heat sink can be expressed as:

$$Q = \dot{m}c_p(T_{w,o} - T_{w,i}) \quad (1)$$

Hence, the experimental convection heat transfer on the cold side can be determined using Newton's law of cooling.

$$h_{exp} = \frac{Q}{A_t(T_{p,c} - T_b)} \quad (2)$$

where,

$$T_b = \frac{T_{w,o} - T_{w,i}}{2} \quad (3)$$

$$A_t = A_f + A_{unf} \quad (4)$$

$$A_{unf} = W \cdot L - N_f \cdot \frac{\pi}{4} d_b^2 \quad (5)$$

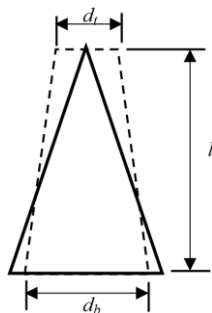


**Figure 8.** Transforming of a cone fin into a truncated cone fin

$$A_f = N_f \frac{\pi}{2} S(d_b + d_t) \quad (6)$$

Figure 8 shows the transformation of a cone shape into a truncated cone while keeping the height constant. Therefore, S can be determined by applying the Pythagorean theorem.

$$S = \sqrt{\left[ l^2 + \left( \frac{d_b - d_t}{2} \right)^2 \right]} \quad (7)$$

A mathematical model has been created to theoretically estimate the outlet temperature of cold water. It balances the energy the heat sink provides and the flowing cold water. The outcomes for  $T_{wo}$  are compared against the experimental data, illustrated in Figure 9.

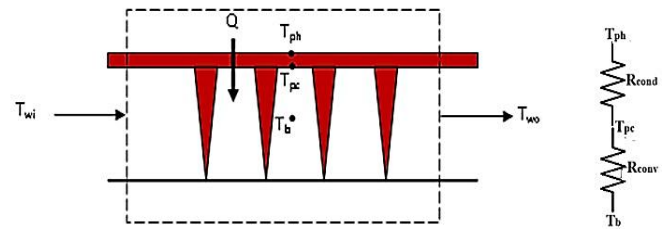


**Figure 9.** A mathematical model of a heat sink

$$Q = \frac{T_{ph} - T_b}{R_{th}} \quad (8)$$

Also,

$$Q = \dot{m}c_p(T_{wo} - T_{wi}) \quad (9)$$

By equating both Eq. (8) and Eq. (9), the result is

$$T_{wo} = \frac{T_{ph} + T_{wi} \left( \frac{1}{2} - I \right)}{\frac{1}{2} + I} \quad (10)$$

where,

$$R_{th} = R_{cond} + R_{conv} \quad (11)$$

$$R_{cond} = \frac{t}{k_c A_p} \quad (12)$$

$$R_{conv} = \frac{1}{\eta_0 h A_t} \quad (13)$$

$$I = \dot{m}c_p R_{th} \quad (14)$$

Khan et al. [35] proposed a correlation to calculate the Nu number in a staggered tube bank, as presented by Grimson [36]. The correlation can be written as follows:

$$Nu = 0.35 F_a Re^{0.57} Pr^{0.31} \quad (15)$$

where,

$$F_a = 1 + 0.1X_l^* + \frac{0.34}{X_t^*} \quad (16)$$

This approach works well for a staggered arrangement! Just remember to change the term  $X_i^{*1.6}$  to  $X_d^{*1.6}$  whenever there's a minimum free-flow area in the diagonal planes of the staggered tube bundle [ $X_l^* < 0.5(2X_t^* + 1)^{\frac{1}{2}}$ ]. Thus,

$$Re = \frac{\rho u_m d_m}{\mu} \quad (17)$$

$$u_m = \frac{X_t^*}{X_t^* - 1} \quad (18)$$

$$X_t^* = \frac{X_t}{d_b} \quad (19)$$

$$X_l^* = \frac{X_l}{d_b} \quad (20)$$

$$X_d^* = \frac{\sqrt{X_t^2 + X_l^2}}{d_b} \quad (21)$$

#### 4. EXPERIMENTAL ANALYSIS OF UNCERTAINTY

It's important to consider that measuring devices have a percentage error, which can vary depending on the accuracy of the manufacturers. As a result, practical test results may have a margin of error. The uncertainty of the measurements must be calculated to ensure confidence in the results. The uncertainty of the experiment was ascertained utilizing the Gaussian distribution principle. The uncertainty (R) is computed using independent variables  $x_1, x_2, \dots, x_n$  and weights  $w_1, w_2, \dots, w_n$ . Consequently, the resulting uncertainty may be suitably evaluated within the established range, which is articulated as [37]:

$$W_R = \left[ \left( \frac{\partial R}{\partial x_1} \times w_1 \right)^2 + \left( \frac{\partial R}{\partial x_2} \times w_2 \right)^2 + \dots + \left( \frac{\partial R}{\partial x_n} \times w_n \right)^2 \right]^{1/2} \quad (22)$$

The measurement device uncertainty in this investigation was calculated using Eq. (21), shown in Table 3.

**Table 3.** The resolution, accuracy, and uncertainties of the utilized measurement devices

Device Name	Resolution	Accuracy	Uncertainty %
Data acquisition Rotameter	0.1°C	0.2°C+2 digit	±0.1117°C
Digital manometer	0.01 MPa	±1.0% of reading or ±1 digit	±0.014388 MPa

#### 5. RESULTS AND DISCUSSION

Following the DOE design working conditions specified in Table 2, a total of 65 experiments were conducted. The EES software was employed to analyze the experimental data, calculating  $q''$ ,  $\Delta T_w$ , Nu,  $V_{con}$ , and  $\Delta P$ . Also, the software was utilized to analyze the parameters above theoretically. Furthermore, the DOE used the experimental data to

investigate the optimal heat sink design between these samples and then experimentally validate their results. The obtained results can be discussed as follows:

#### 5.1 Heat flux

EES software is used to analyze experimental heat fluxes for all experiments according to the working conditions in Table 2. The results are expressed in Figure 10. It is indicated that the highest  $q''$  occurred in  $\beta$  of 0 compared to others in all working conditions due to the reduction of the contact surface area between the base plate of the heat sink and the fin base. As is known, the principles of conduction heat transfer in materials depend on three parameters: Temperature difference, thermal conductivity, and cross-sectional area perpendicular to the heat flow direction. It also showed how the working conditions influence the rate of heat transfer. It showed that  $q''$  values depend on the steam pressure and cold-water flow rate, in addition to the fin geometry. The heights  $q''$  was obtained when working conditions were at P5V3, while they decreased when steam pressure decreased. They ranged from 32800 to 10700 when working conditions changed from P5V3 to P2V1, respectively. It was observed that as the fin shape changed after a  $\beta$  value of 0.4, the decrease in contact area reduced the conduction heat transfer from the plate to the fin. Additionally, there was an increased convection resistance in the non-finned heat sink area. Consequently, the minimum  $q''$  occurred at a  $\beta$  value of 0.8, ranging from 8170 to 20650 W/m<sup>2</sup> as the working conditions transitioned from P2V1 to P3V4.

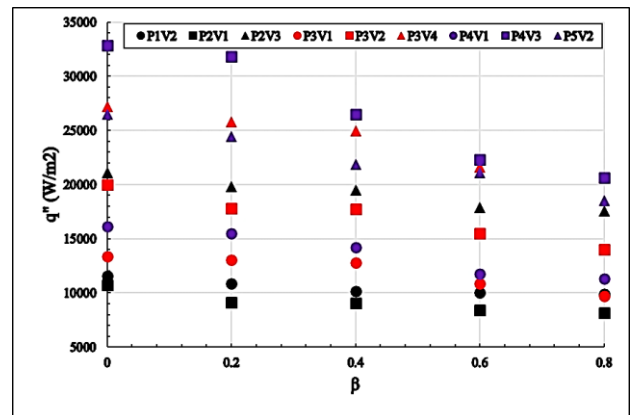


**Figure 10.** The variation of heat flux in relation to  $\beta$  for the experiments

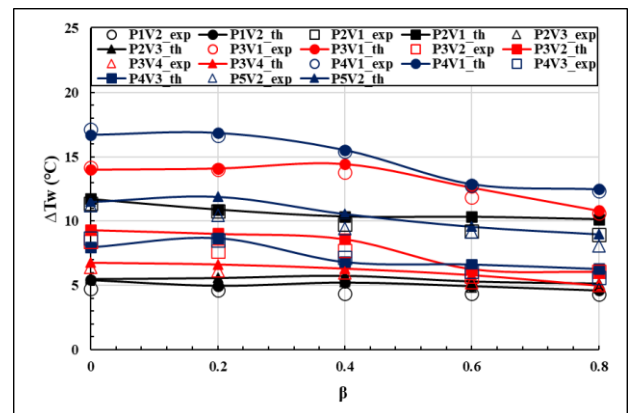


**Figure 11.** Experimental and theoretical outlet water temperature variation vs.  $\beta$

## 5.2 The outlet water temperature

The exit cold water from the condensing chamber was theoretically estimated using the mathematical model depicted in Figure 9 and validated with experimental data from all experiments. The results are presented in Figure 11. It indicates there is good agreement between theoretical and experimental data; in most cases, there is matching between them. The error percentage in 12 of 65 experiments was less than 1%, and only in two of these experiments did the error percentage exceed 8%. In other cases, the error percentage ranged from 1% to 5%, indicating that the theoretical and experimental data have been in good agreement. The validation results indicated that experiments have been conducted in a steady state condition.

## 5.3 Convection heat transfer coefficient

The Nu number was determined experimentally, and the results shown in Figure 12 indicate that it decreases as  $\beta$  increases. The cold-water flow rate categorizes the Nu number into three groups based on steam pressure across different ranges. This is due to the significant impact of the water mass flow rate on the heat transfer rate. The Nu numbers in each group were closely together, regardless of the steam pressure values that differed in experiments. In the experiments with a water flow rate of V3, the Nu numbers ranged from an average of 8 to 4.5. For the V2 experiments, the Nu numbers ranged from 6 to 4; in the V1 experiments, they ranged from 4.3 to 2.5. Each practical experiment was repeated ten times, and the average was used in the analysis data. The standard error bars display errors in the Nu number for each experiment, which does not exceed 5% as shown in Figure 12.

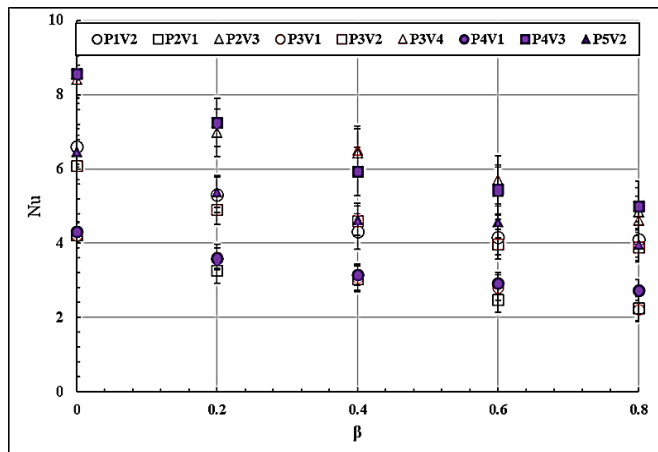


Figure 12. The relation between Nu number and Beta for experiments

## 5.4 The formation process of steam condensing

In an ordinary thermal system, steam condensation depends on two main factors: steam pressure and cooling surface temperature. In the present study, the fin shape factor of a heat sink system is added to two previous factors to examine its effect on steam condensation. In the experiments, the volumetric rate of condensing steam in the condensing chamber was measured in addition to studying the performance of the heat sink types, as shown in Figure 13. It indicates a significant effect of the fin shape on the condensing steam, resulting from heat sink dissipation. It was found that

the maximum steam condensation was at  $\beta$  of 0 in all experiments, similar to a heat transfer rate, and then decreased when  $\beta$  increased. It has been observed that the steam condensation rates in both P1V2 and P2V1 match; it exhibits the lowest condensation compared to other operating conditions. The condensation rates were similar for all fin shapes, except at a  $\beta$  value of 0.4, where the difference between them was approximately 1.04 cm/min. When the working conditions changed, the steam condensation rate varied depending on the cold-water flow rate and steam pressure, with the highest condensation rate occurring at P4V3. The difference in condensation between it and P5V2 decreased when the fin shape was changed, and they became approximately matched at 0.8.

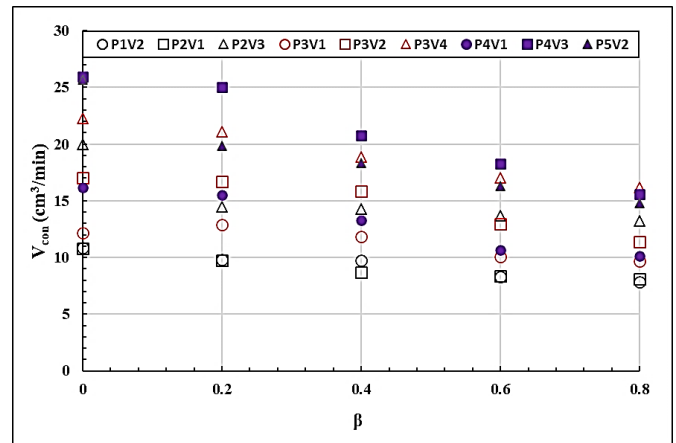


Figure 13. The experimental steam condensation rate in relation to the  $\beta$  factor

## 5.5 Pressure drop

Figure 14 shows the pressure drop variation in the experiments conducted. It was observed to have an insignificant impact on the fin shape change.

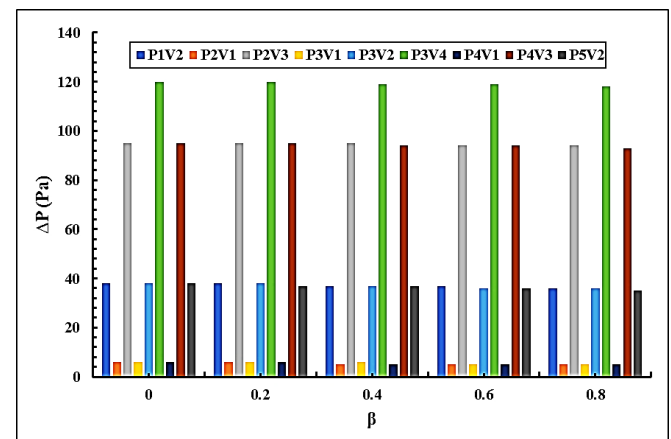


Figure 14. Pressure drop behavior in experiments

This was due to the experiments being performed at low Re numbers and limiting the change in the thermophysical properties of cold water because the change in water temperature variation was not large. Regardless of steam pressure values, the Re numbers varied from 8 to 60 for a water flow rate of 0.5 to 2.25 LPM, respectively. Since the pressure drop majorly depends on the Re number, no pressure drop was noted at the fin change shape for the same water flow rate. In

all experiments conducted, the limit of pressure drop corresponding to water flow was observed as 6, 38, 95, and 120 Pa for 0.5, 1.25, 2, and 2.25 LPM, respectively.

### 5.6 Optimum experiment design

The experiment data was inserted into the DOE software to obtain the best possible conditions for each variable. The program determined the optimal conditions for each case based on a composite desirability factor ranging from 0.998 to

0.999, so the experiments have been conducted accordingly to it. Table 4 presents the optimum experimental working conditions for each  $\beta$  case in both methods. The results indicate a close match between the two sets of data. The error ratio between the results ranged from 1.3% to 12% across three parameters. Additionally, as indicated in Table 5, DOE software recommended a set of correlation relations to assess the rate of heat transfer, pressure drop, and steam condensation as a function of steam pressure and water flow rate for each case.

**Table 4.** Data on optimum working conditions suggested by Minitab and experimental work

$\theta$	$\beta$	Working Conditions		DOE Optimization Results			Experimental Work Results		
		Ps (Pa)	Vw (LPM)	Q (W)	$\Delta P$ (Pa)	Vcon (cm <sup>3</sup> /min)	Q (W)	$\Delta P$ (Pa)	Vcon (cm <sup>3</sup> /min)
	0	7833.33	2.03	898.51	99.2	23.93	928.4	95.12	24.42
	0.2	8944.44	2	899.92	98.88	23.766	887.9	95	24.21
30	0.4	11500	1.225	707.65	35.81	17.987	693.3	37	18.31
	0.6	5055	2.145	624.9	113.9	16.016	613.6	95	15.48
	0.8	10833.33	1.7727	599.7	74.77	14.85	629.1	76	16.8

**Table 5.** List of correlation equations to calculate Q,  $\Delta P$ , and Vcon as functions of Ps and Vw, suggested by Minitab

$\beta$	Correlation Equation	R <sup>2</sup> %
0	$Q = 306.637 + 49.9843 V_w + 0.00439911 P_s + 57.063 V_w^2 + 1.32516 \times 10^{-6} P_s^2 + 0.019425 P_s V_w$ $\Delta P = -5.56073 + 12.8792 V_w + 2.06808 \times 10^{-4} P_s + 19.1055 V_w^2 - 1.7234 \times 10^{-8} P_s^2 + 3.82962 \times 10^{-18} P_s V_w$ $V_{con} = 5.63288 + 4.14399 V_w + 6.577418 \times 10^{-4} P_s + 0.75374 V_w^2 + 3.18667 \times 10^{-9} P_s^2 + 4.25 \times 10^{-4} V_w P_s$	88.21 99.97 89.65
0.2	$Q = 227.217 + 93.8789 V_w + 0.018984 P_s + 42.7907 V_w^2 - 2.97738 \times 10^{-7} P_s^2 + 0.01755 P_s V_w$ $\Delta P = -4.38413 + 10.1749 V_w + 1.92545 \times 10^{-4} P_s + 19.9029 V_w^2 - 1.60454 \times 10^{-8} P_s^2 + 1.97668 \times 10^{-19} P_s V_w$ $V_{con} = 9.14734 + 0.214081 V_w + 7.98508 \times 10^{-5} P_s + 2.29905 V_w^2 + 5.43418 \times 10^{-8} P_s^2 + 3.41667 \times 10^{-4} V_w P_s$	98.11 99.98 95.29
0.4	$Q = 99.3535 + 304.014 V_w + 0.0372598 P_s - 44.6922 V_w^2 - 2.91984 \times 10^{-6} P_s^2 + 20.95 \times 10^{-3} P_s V_w$ $\Delta P = 8.07044 - 7.63831 V_w - 6.35046 \times 10^{-4} P_s + 18.6869 V_w^2 - 1.27175 \times 10^{-7} P_s^2 + 2.5 \times 10^{-3} P_s V_w$ $V_{con} = 4.26938 + 7.50605 V_w + 9.35478 \times 10^{-4} P_s - 0.937231 V_w^2 - 5.3287 \times 10^{-8} P_s^2 + 41.6667 \times 10^{-5} V_w P_s$	94.04 97.56 88.65
0.6	$Q = 437.747 - 114.342 V_w - 0.0240821 P_s + 101.963 V_w^2 + 2.76731 \times 10^{-6} P_s^2 + 0.012375 P_s V_w$ $\Delta P = -1.79471 + 4.50275 V_w + 6.41817 \times 10^{-5} P_s + 21.7454 V_w^2 - 5.34848 \times 10^{-9} P_s^2 + 5.14145 \times 10^{-19} P_s V_w$ $V_{con} = 15.528 - 6.32207 V_w - 6.2072 \times 10^{-4} P_s + 3.77391 V_w^2 + 6.89225 \times 10^{-8} P_s^2 + 37.5 \times 10^{-5} V_w P_s$	92.54 100 88.1
0.8	$Q = 259.451 + 89.1996 V_w + 6.37759 \times 10^{-3} P_s + 37.0424 V_w^2 + 4.89825 \times 10^{-7} P_s^2 + 6.15833 \times 10^{-3} P_s V_w$ $\Delta P = -0.932229 + 2.16667 V_w + 7.20382 \times 10^{-5} P_s + 22.6667 V_w^2 - 1.09014 \times 10^{-22} P_s^2 - 8.33333 \times 10^{-5} P_s V_w$ $V_{con} = 14.1224 - 2.28698 V_w - 3.83921 \times 10^{-4} P_s + 1.52234 V_w^2 + 3.13282 \times 10^{-8} P_s^2 + 41.6667 \times 10^{-5} V_w P_s$	94.38 100 96.91

## 6. CONCLUSIONS

The study investigated how changing the fin shape of a heat sink from a cone to a truncated cone affects its thermal performance. This transformation was also tested in steam condensation experiments to determine the most effective heat sink design. The fin shape was altered while maintaining the same fin length, lateral surface area, and transverse pitch. Experimental tests were designed using DOE software to analyze two input variables and select a response surface. As a result, 13 tests should be performed for each  $\beta$  case. The present study investigated five fin shapes based on the  $\beta$  factor ranging from 0 to 0.8 under laminar convection heat transfer conditions. The most prominent findings of the study are listed below:

- Changing the cone fin to a truncated cone decreases the heat sink thermal performance, which decreases even more as the  $\beta$  factor increases. This is due to a decrease in the contact surface area between the fin base and plate surface, which decreases the heat conduction surface area and increases the heat convection surface area.

- The results from experiments clearly show that changing the shape of the conical fin to a truncated cone fin significantly affects the heat transfer coefficient. However, the theoretical method indicates that this change has little effect, likely due to

the low Re number and slight variation in cold water. This is consistent with the findings of Ahmadian-Elmi et al. [38], which conducted a similar numerical study under forced conditions and with different cone fin dimensions.

- Based on the study's results, truncated conical fins should be avoided in the production of heat sinks due to their lower thermal performance compared to conical fins.

## REFERENCES

- [1] Lee, H. (2022). Thermal Design: Heat Sinks, Thermoelectrics, Heat Pipes, Compact Heat Exchangers, and Solar Cells. John Wiley & Sons.
- [2] Harper, R.R., Brown, W.B. (1923). Mathematical equations for heat conduction in the fins of air-cooled engines. National Advisory Committee for Aeronautics, No. NACA-TR-158.
- [3] Doetsch, H. (1934). Die Wärmeübertragung von Kühlrippen an strömende Luft. Abhandlungen Aus Dem Aerodynamischen Institut an Der Technischen Hochschule Aachen. [https://doi.org/10.1007/978-3-642-94173-3\\_1](https://doi.org/10.1007/978-3-642-94173-3_1)
- [4] Kraus, A.D., Aziz, A., Welty, J. (2002). Extended Surface Heat Transfer. John Wiley & Sons.

- [5] Abbas, E.F. (2021). An analytical and experimental evaluation of a heat sink under constant heat flow and forced convection heat transfer. *Journal of Engineering and Technological Sciences*, 53(4): 210405. <https://doi.org/10.5614/j.eng.technol.sci.2021.53.4.5>
- [6] Abbas, E.F., Jassim, A.H., Salem, T.K. (2023). Review of the fin optimization in the heat sink design. *International Review of Mechanical Engineering*, 17(10): 478. <https://doi.org/10.15866/ireme.v17i10.23824>
- [7] Gardner, K.A. (1945). Efficiency of extended surface. *Transactions of the American Society of Mechanical Engineers*, 67(8): 621-628. <https://doi.org/10.1115/1.4018343>
- [8] Snider, A.D., Kraus, A.D. (1987). The quest for the optimum longitudinal fin profile. *Heat Transfer Engineering*, 8(2): 19-25. <https://doi.org/10.1080/01457638708962790>
- [9] Razelos, P., Imre, K. (1983). Minimum mass convective fins with variable heat transfer coefficients. *Journal of the Franklin Institute*, 315(4): 269-282. [https://doi.org/10.1016/0016-0032\(83\)90078-9](https://doi.org/10.1016/0016-0032(83)90078-9)
- [10] Aziz, A., Beers-Green, A.B. (2009). Performance and optimum design of convective-radiative rectangular fin with convective base heating, wall conduction resistance, and contact resistance between the wall and the fin base. *Energy Conversion and Management*, 50(10): 2622-2631. <https://doi.org/10.1016/j.enconman.2009.06.017>
- [11] Hempijid, T., Kittichaikarn, C. (2020). Effect of heat sink inlet and outlet flow direction on heat transfer performance. *Applied Thermal Engineering*, 164: 114375. <https://doi.org/10.1016/J.APPLTHERMALENG.2019.114375>
- [12] Peng, M., Chen, L., Ji, W., Tao, W. (2020). Numerical study on flow and heat transfer in a multi-jet microchannel heat sink. *International Journal of Heat and Mass Transfer*, 157: 119982. <https://doi.org/10.1016/j.ijheatmasstransfer.2020.119982>
- [13] Sehgal, S.S., Murugesan, K., Mohapatra, S.K. (2009). Effect of flow arrangements on thermohydraulic performance of a microchannel heat sink. *International Conference on Micro/Nanoscale Heat Transfer*, 43918: 13-19. <https://doi.org/10.1115/MNHMT2009-18016>
- [14] Babar, H., Wu, H., Ali, H.M., Zhang, W. (2023). Hydrothermal performance of inline and staggered arrangements of airfoil shaped pin-fin heat sinks: A comparative study. *Thermal Science and Engineering Progress*, 37: 101616. <https://doi.org/10.1016/j.tsep.2022.101616>
- [15] Leon, O.A., De Mey, G., Dick, E., Vierendeels, J. (2004). Staggered heat sinks with aerodynamic cooling fins. *Microelectronics Reliability*, 44(7): 1181-1187. <https://doi.org/10.1016/J.MICROREL.2004.03.003>
- [16] Abuşka, M., Çorumlu, V. (2023). A comparative experimental thermal performance analysis of conical pin fin heat sink with staggered and modified staggered layout under forced convection. *Thermal Science and Engineering Progress*, 37: 101560. <https://doi.org/10.1016/j.tsep.2022.101560>
- [17] Yoo, S.Y., Kwon, H.K., Kim, J.H. (2007). A study on heat transfer characteristics for staggered tube banks in cross-flow. *Journal of Mechanical Science and Technology*, 21: 505-512. <https://doi.org/10.1007/BF02916312>
- [18] Achenbach, E. (1989). Heat transfer from a staggered tube bundle in cross-flow at high Reynolds numbers. *International Journal of Heat and Mass Transfer*, 32(2): 271-280. [https://doi.org/10.1016/0017-9310\(89\)90174-9](https://doi.org/10.1016/0017-9310(89)90174-9)
- [19] John, T., Mathew, B., Hegab, H. (2010). Characteristic study on the optimization of micro pin-fin heat sink with staggered arrangement. In *10th AIAA/ASME Joint Thermophysics and Heat Transfer Conference*, Chicago, Illinois, pp. 4781. <https://doi.org/10.2514/6.2010-4781>
- [20] Tekale, H.M., Pawar, R.S., Deshmukh, D.A. (2020). Experimental investigation of heat transfer enhancement in solid cylindrical & cylindrical with perforated fins in staggered & in inline arrangements. *International Journal for Modern Trends in Science and Technology*, 6(5): 139-161. <https://doi.org/10.46501/ijmst060524>
- [21] Maji, A., Bhanja, D., Patowari, P.K. (2017). Numerical investigation on heat transfer enhancement of heat sink using perforated pin fins with inline and staggered arrangement. *Applied Thermal Engineering*, 125: 596-616. <https://doi.org/10.1016/j.applthermaleng.2017.07.053>
- [22] Choudhary, V., Kumar, M., Patil, A.K. (2019). Experimental investigation of enhanced performance of pin fin heat sink with wings. *Applied Thermal Engineering*, 155: 546-562. <https://doi.org/10.1016/j.applthermaleng.2019.03.139>
- [23] bin Samsudin, A.N., Tijani, A.S., Abdulrahman, S.T., Kubenthiran, J., Muritala, I.K. (2023). Thermal-hydraulic modeling of heat sink under force convection: Investigating the effect of wings on new designs. *Alexandria Engineering Journal*, 65: 709-730. <https://doi.org/10.1016/J.AEJ.2022.10.045>
- [24] Abdelmohimen, M.A., Hussien, M.A., Algarni, S., Karali, M.A., Saleel, C.A., Ahmed, G.M., Refaey, H.A. (2024). Numerical investigation of thermal performance enhancement of pin fin heat sink using wings with different angles. *Ain Shams Engineering Journal*, 15(3): 102584. <https://doi.org/10.1016/j.asej.2023.102584>
- [25] Qi, X., Wang, L., Qing, T., Yang, P., Liu, Y. (2024). Study on thermo-hydraulic performance and correlation development of the interrupted flying-wing fins. *ASME Journal of Heat and Mass Transfer*, 146(3): 031002. <https://doi.org/10.1115/1.4063964>
- [26] Massoudi, M.D., Hamida, M.B.B. (2023). Combined impacts of square fins fitted wavy wings and micropolar magnetized-radiative nanofluid on the heat sink performance. *Journal of Magnetism and Magnetic Materials*, 574: 170655. <https://doi.org/10.1016/j.jmmm.2023.170655>
- [27] Haque, M.R., Hridi, T.J., Haque, M.M. (2022). CFD studies on thermal performance augmentation of heat sink using perforated twisted, and grooved pin fins. *International Journal of Thermal Sciences*, 182: 107832. <https://doi.org/10.1016/j.ijthermalsci.2022.107832>
- [28] Miao, L., Wan, R., Wu, H.W., Liu, Z., Wang, S.S. (2023). Heat transfer and pressure drop characteristic research of sine wavy flying-wing fins. *Scientific Reports*, 13(1): 15589. <https://doi.org/10.1038/s41598-023-42872-x>
- [29] Çorumlu, V. (2024). The effects of input power and ambient temperature on the thermal performance of conical pin fin heat sink in natural convection.

International Journal of Thermal Sciences, 197: 108855.  
<https://doi.org/10.1016/j.ijthermalsci.2023.108855>

- [30] Ho, J.Y., Leong, K.C. (2020). Effect of fin pitch on the filmwise condensation of steam on three-dimensional conical pin fin arrays: A comparative study. International Journal of Heat and Mass Transfer, 150: 119328. <https://doi.org/10.1016/j.ijheatmasstransfer.2020.119328>
- [31] Haghghi, S.S., Goshayeshi, H.R., Zahmatkesh, I. (2024). Experimental investigation of forced convection heat transfer for different models of PPFHS heatsinks with different fin-pin spacing. Heliyon, 10(1): e23373. <https://doi.org/10.1016/j.heliyon.2023.e23373>
- [32] Jaiswal, L., Hassan, M.U., Kumar, A. (2018). Experimentation and thermal analysis of cylindrical and conical shaped fins. International Journal of Mechanical Engineering, 7(4): 1-10.
- [33] Souida, S., Sahel, D., Ameer, H., Yousfi, A. (2022). Numerical simulation of heat transfer behaviors in conical pin fins heat sinks. Acta Mechanica Slovaca, 26(3): 32-41. <https://doi.org/10.21496/ams.2023.002>
- [34] Pati, B., Sharma, B., Palo, A., Barman, R.N. (2018). Numerical investigation of pin-fin thermal performance for staggered and inline arrays at low Reynolds number. International journal of Heat and Technology, 36(2): 697-703. <https://doi.org/10.18280/ijht.360235>
- [35] Khan, W.A., Culham, J.R., Yovanovich, M.M. (2006). Analytical model for convection heat transfer from tube banks. Journal of Thermophysics and Heat transfer, 20(4): 720-727. <https://doi.org/10.2514/1.15453>
- [36] Grimison, E.D. (1937). Correlation and utilization of new data on flow resistance and heat transfer for cross flow of gases over tube banks. Transactions of the American Society of Mechanical Engineers, 59(7): 583-594. <https://doi.org/10.1115/1.4020557>
- [37] Figliola, R.S., Beasley, D.E. (2021). Theory and Design for Mechanical Measurements, International Adaptation. John Wiley & Sons.
- [38] Ahmadian-Elmi, M., Mashayekhi, A., Nourazar, S.S., Vafai, K. (2021). A comprehensive study on parametric optimization of the pin-fin heat sink to improve its thermal and hydraulic characteristics. International Journal of Heat and Mass Transfer, 180: 121797. <https://doi.org/10.1016/J.IJHEATMASSTRANSFER.2021.121797>

## NOMENCLATURE

$A_b$	Base diameter, m <sup>2</sup>
$A_f$	Lateral surface area of the fin, m <sup>2</sup>
$A_p$	Cross-section area of the base plate, m <sup>2</sup>
$A_t$	Total area, m <sup>2</sup>
$A_{unf}$	Non-finned area, m <sup>2</sup>
$c_p$	Specific heat J.kg <sup>-1</sup> . °C <sup>-1</sup>
$d_b$	Base diameter, m
$d_m$	Mean diameter, m
$d_t$	Tip diameter, m
$h_{exp}$	Experimental convection heat transfer coefficient, W.m <sup>-2</sup> .°C <sup>-1</sup>
$k_c$	Thermal conductivity of copper, W.m <sup>-1</sup> .°C <sup>-1</sup>
$k_w$	Thermal conductivity of copper, W.m <sup>-1</sup> .°C <sup>-1</sup>
$l$	Fin length, m
$L$	Length of the base plate, m
$\dot{m}$	Mass flow rate, kg.s <sup>-1</sup>
$N_f$	Number of fins
$\Delta P$	Pressure drop, Pa
$R_{cond}$	Conduction thermal resistance, °C.W <sup>-1</sup>
$R_{conv}$	Convection thermal resistance, °C.W <sup>-1</sup>
$R_{th}$	Total thermal resistance, °C.W <sup>-1</sup>
$S$	Fin circumference, m
$t$	Thickness of the base plate, m
$T_b$	Bulk temperature, °C
$T_{p,c}$	Cold side plate temperature, °C
$T_{p,h}$	Hot side plate temperature, °C
$T_{w,i}$	Cold water inlet temperature, °C
$T_{w,o}$	Cold water outlet temperature, °C
$u_m$	Maximum water velocity, m.s <sup>-1</sup>
$V_{con}$	Volumetric rate of condensation, cm <sup>3</sup> .min <sup>-1</sup>
$V_w$	Volumetric rate of water, LPM
$W$	Width of the base plate, m
$X_d$	Diagonal pitch, m
$X_l$	Lateral pitch, m
$X_t$	Transverse pitch, m
$Nu$	Nusselt number
$Pr$	Prandtl number
$Re$	Reynolds number

## Greek symbols

$\rho$	Density of the water, kg.m <sup>-3</sup>
$\mu$	Viscosity of the water, kg.m <sup>-1</sup> .s <sup>-1</sup>